physica status solidi a
www.pss-a.com

Synthesis, Characterization, and Optical Properties of New Organic–Inorganic Hybrid Perovskites $[(NH_3)_2(CH_2)_3]CuCl_4$ and $[(NH_3)_2(CH_2)_4]CuCl_2Br_2$

Seham K. Abdel-Aal, Mohamed F. Kandeel, Ashraf F. El-Sherif, and Ahmed S. Abdel-Rahman**

Organic–inorganic hybrid perovskites (OIHs) are exceptionally promising sector of novel materials for optoelectronic applications. Herein, the OIHs of the formula $[(NH_3)_2(CH_2)_3]CuCl_4$ labeled by C_3CuCl and $[(NH_3)_2(CH_2)_4]CuCl_2Br_2$ labeled by $C_4CuClBr$ are prepared by slow evaporation method. The synthesis process is achieved by mixing equimolar ethanolic solutions ratios (1:1) of their basic components (organic/inorganic). Characterizations of these materials using microchemical analysis, energy dispersion X-ray (EDX) and X-ray diffraction (XRD) are discussed. The XRD is used to estimate the crystalline size for prepared compounds and found in the range of 38.8 and 48.8 nm for C_3CuCl and $C_4CuClBr$, respectively. The vibrational spectra are studied by Fourier transformation infrared spectroscopy (FTIR) and show the major diffraction peaks of compounds and their assignment. UV-region strong absorption is clarified in the optical properties studied for Cu hybrid, whereas the bandgap energy estimated via Kubelka–Munk equation and found 2.8 and 3.85 eV for C_3CuCl and $C_4CuClBr$, respectively.

1. Introduction

In the Ural Mountains of Russia, Gustav Rose, in 1839, has discovered the perovskite and named afterward by L. A. Perovski (1792–1856), the Russian mineralogist, all materials of the crystal structure similar to $CaTiO_3$.[1] Perovskites are one of the most important groups in material science due to their extraordinary physical and chemical properties. As it has properties appropriate for many uses, the perovskite architecture has and continues to attract interest.[2]

Dr. S. K. Abdel-Aal, Dr. A. S. Abdel-Rahman
Physics Department
Faculty of Science
Cairo University
12613 Cairo, Egypt
E-mail: seham@sci.cu.edu.eg; asabry@sci.cu.edu.eg

M. F. Kandeel, Prof. A. F. El-Sherif
Laser and Photonics Center
Engineering Physics Department
Military Technical College
Cairo, Egypt

The ORCID identification number(s) for the author(s) of this article can be found under https://doi.org/10.1002/pssa.202100036.

DOI: 10.1002/pssa.202100036

Organic–inorganic hybrid perovskites (OIHPs) of the formula ABX_4 where A represents the organic diamine cation, B represents the metal ion, and X is the halogen (I, Br, Cl, and so on) are class of new materials that have very promising applications[2–8] and tunable properties and structure. Many scientists are attracted to work in OIHPs applications in photonics, other fields and the preliminary speculation was accompanied by work into the mechanical, optical, and structural properties of perovskites. Perovskites collect characteristics of both inorganic and organic: chemical tuning of their optoelectronic properties, minimal-temperature solution-based organic deposition remembrance.[7–9]

Bandgap is of crucial importance in optoelectronic applications. It is the best-known feature of hybrid perovskites where their bandgap can be broadly modified from blue-to-red spectral areas. It is possible to adjust the energy gap in hybrid perovskites by adjusting the perovskites geometry. Geometry tuning can be accomplished by changing temperature and eliminating perovskite components.[4] This scope is accomplished by adding the halide, increasing the width of the chain or both. The inorganic octahedron holds the valence and conduction bands. The valence band comprises hybridized metal and halide p-orbitals, whereas the conductive band is mostly distinguished by small contributions from the orbital halides.[5,6] These bands found to be independent on the organic cation but modulate the bandgap by changing the bond length of metal-halide,[10] which ensures that the shifts generated by removing the organic cation are less noticeable than those created by halide replacement.

The hybrid perovskites of the formula A_2MX_4, A: ammonium-substituted organic cation, M: a divalent metal ion, and X: a halogen (Cl, Br, I) like the presently investigated hybrid perovskite of $[(NH_3)_2(CH_2)_3]CuCl_4$ and $[(NH_3)_2(CH_2)_4]CuCl_2Br_2$. The crystal structure of these hybrid perovskites is stabilized by a series of hydrogen bonds and van der Waals interactions between anions and cations. The ammonium ion at the end of organic chains forms N–H···X hydrogen bonds with the halide ion of the metallic layer. The structure of inorganic layer of Cu hybrid as reported before[11–17] consists of corner-shared octahedral distorted $[CuCl_4]^{2-}$ anion alternative with organic layer $[(NH_3)_2(CH_2)_n]^2$ cations.

To save the environment and solve the energy crisis, it is important to use environmental friendly, low-cost, and lead-free materials in perovskite solar cell applications, all these requirements are involved in the Cu hybrid perovskite that are previously reported.[11–18] As the optical properties of lower organic chain length of Cu hybrid perovskite is not reported as well as introducing of both Cl and Br ion in lower chain lengths. It is of our interest to prepare and study some of the properties of C_3CuCl and $C_4CuClBr$ to add to global knowledge about these promising materials.

2. Experimental Section

2.1. Synthesis

All used chemicals in the preparations are used as-received and purchased from Sigma-Aldrich with purity exceeds 97%. All solvents were of reagent grade.

2.1.1. Synthesis of $[(NH_3)_2(CH_2)_3]CuCl_4$ Hybrid Perovskites

The organic cation $[(NH_3)_2(CH_2)_3]Cl_2$ 1,2 diamine propane-chlorate was prepared according to the previous works.[18–21]

The $[(NH_3)_2(CH_2)_3]CuCl_4$ was prepared by mixing the ethanolic solution of organic cation and $CuCl_2$ in 1:1 ratio with constant stirring, heat (60 °C for 30 min) and then slow cooling to room temperature. The steps of preparation are indicated in **Figure 1**. Green powder of $[(NH_3)_2(CH_2)_3]CuCl_4$ denoted C_3CuCl precipitate out, as shown in **Figure 2**. The reaction equation is

$$[(NH_3)_2(CH_2)_3]Cl_2 + CuCl_2 \xrightarrow{\Delta} [(NH_3)_2(CH_2)_3]CuCl_4 \quad (1)$$

2.1.2. Synthesis of $[(NH_3)_2(CH_2)_4]CuCl_2Br_2$ Hybrid Perovskites

The organic cation 1,4 diamine butane bromide $[(NH_3)_2(CH_2)_4]Br_2$ synthesized by the same method of $[(NH_3)_2(CH_2)_3]Cl_2$ using HBr. The salt was filtered, washed with alcohol, and used.[20,22,23]

The perovskite hybrid of $[(NH_3)_2(CH_2)_4]CuCl_2Br_2$ was prepared according to Equation (2).[11,20,24] The steps of preparation are shown in **Figure 3**. Brown cubic crystals of $[(NH_3)_2(CH_2)_4]CuCl_2Br_2$ denoted $C_4CuClBr$ precipitate out, as shown in **Figure 4**.

$$[(NH_3)_2(CH_2)_4]Br_2 + CuCl_2 \xrightarrow{\Delta} [(NH_3)_2(CH_2)_4]CuCl_2Br_2 \quad (2)$$

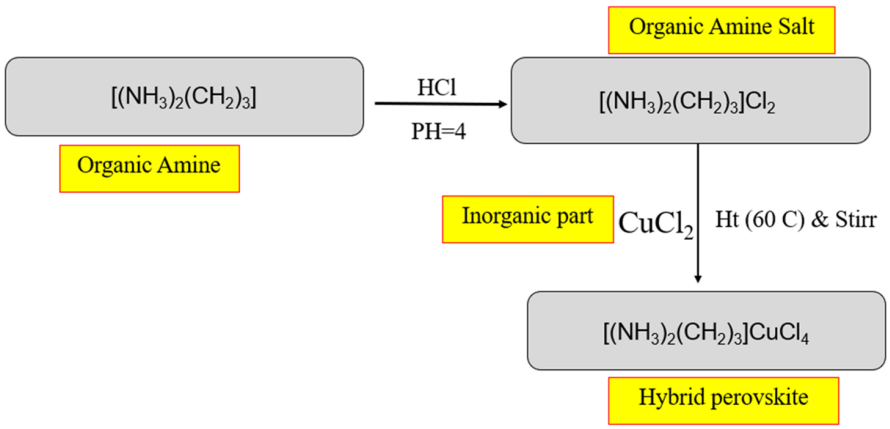

Figure 1. OIHPs procedure of C_3CuCl.

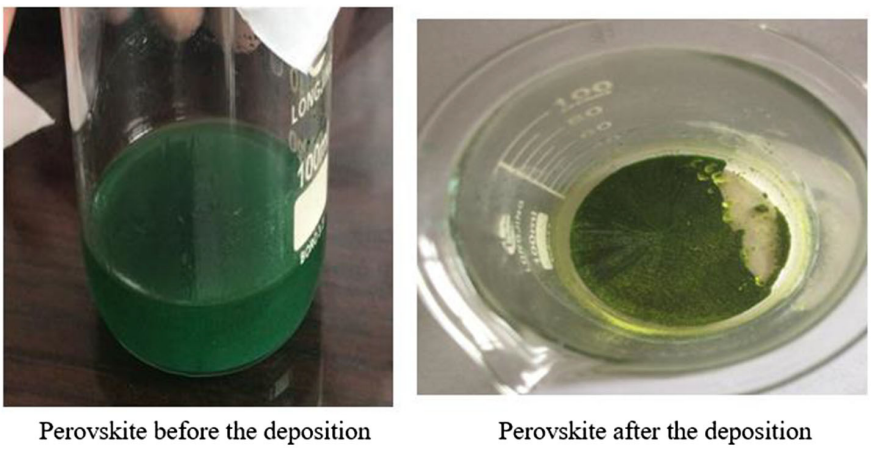

Figure 2. C_3CuCl perovskite before and after the deposition.

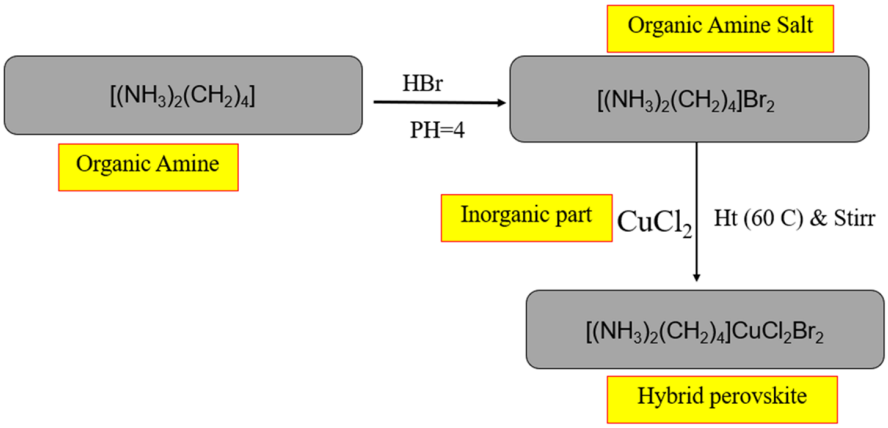

Figure 3. OIHPs procedure of $C_4CuClBr$.

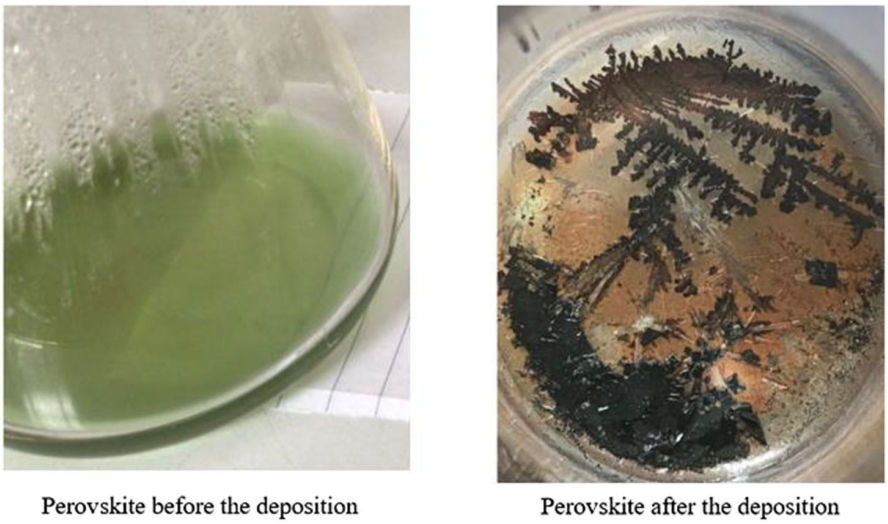

Figure 4. Indicate the $C_4CuClBr$ perovskite before and after the precipitation.

2.2. Characterizations

2.2.1. Elemental Analysis

Carbon, hydrogen, and nitrogen microchemical analysis carried out in a Perkin Elmer C,H,N analyzer and energy-dispersive X-ray (EDX) spectroscopy was carried out on samples by scanning electron microscope (SEM) equipped with an EDX detector type SUTW-Sapphire, resolution:132.14 and was operating at 25 kV.

2.2.2. X-Ray Powder Diffraction Measurement

The X-ray powder diffractometer Siemens D-500 computer controlled with Cu Kα radiation $\lambda = 1.54056$ Å were used to collect XRD powder diffraction data with the measuring range (2θ) from 5° to 70°, step 0.04.

2.2.3. Infrared Spectroscopy (IR)

The Fourier transformation infrared (FTIR) spectroscopy measurements were achieved on FTIR 4100 spectrometer using pure KBr pellets and the measuring spectra in the range 4000–400 cm^{-1}.

Table 1. The chemical analysis of synthesized perovskites.

Compound	Elements					
	Measured			Calculated		
	C%	H%	N%	C%	H%	N%
C_3CuCl	13.46	5.52	10.96	12.79	4.26	9.95
$C_4CuClBr$	12.36	3.76	7.85	12.49	3.71	7.29

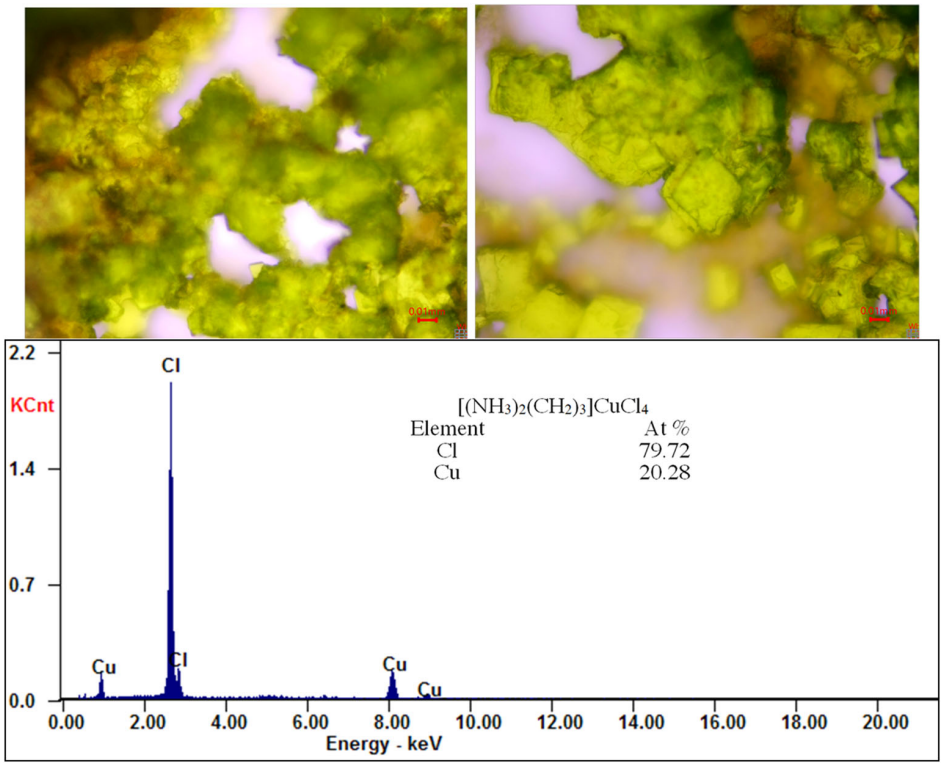

Figure 5. Crystal image and EDX spectrum of C_3CuCl.

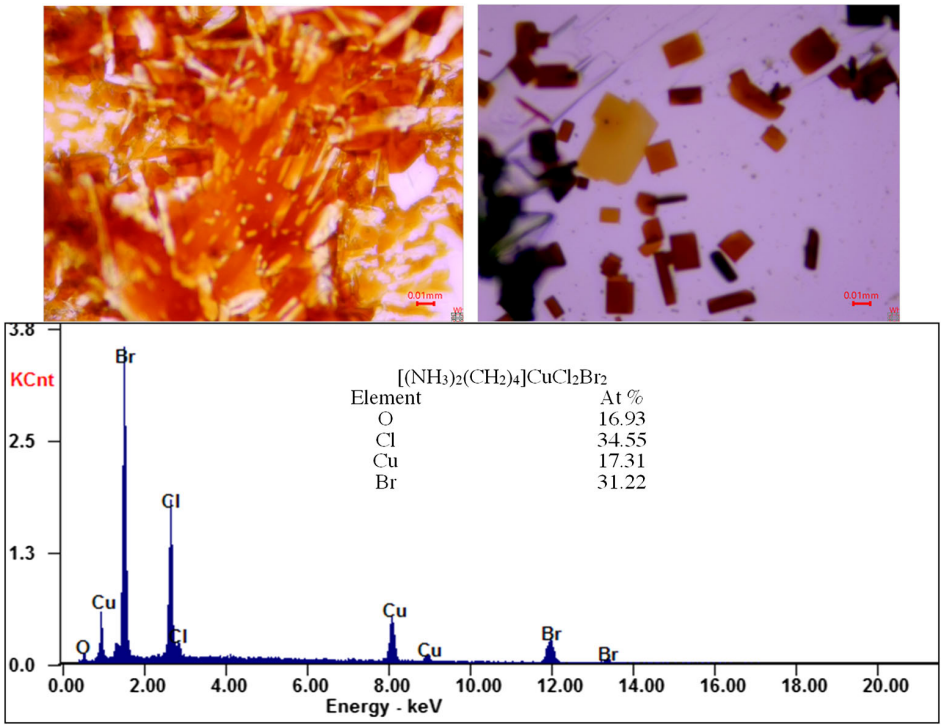

Figure 6. Crystal image and EDX spectrum of $C_4CuClBr$.

2.2.4. Optical Properties

Jenway 7205 UV–vis Scanning Spectrometer was used in measurements of optical properties of the samples and collects data from 200 to 2000 nm wavelength range.

Table 2. The average bond length of $[(NH_3)(CH_2)_n(NH_3)]CuX_4$, $n = 2, 3, 4.$, X = Cl, Br.

Chemical formula		Average metal–halogen bond length	References
$[(NH_3)(CH_2)_2(NH_3)]CuCl_4$	C2CuCl	Cu—Cl = 2.312 Å	[30]
$[(NH_3)(CH_2)_2(NH_3)]CuBr_4$	C2CuBr	Cu—Br = 2.436 Å	[31]
$[(NH_3)(CH_2)_3(NH_3)]CuCl_4$	C_3CuCl	Cu—Cl	No available data
$[(NH_3)(CH_2)_3(NH_3)]CuBr_4$	C_3CuBr	Cu—Br = 2.441 Å	[31]
$[(NH_3)(CH_2)_4(NH_3)]CuCl_4$	C_4CuCl	Cu—Cl = 2.294 Å	[20]
$[(NH_3)(CH_2)_4(NH_3)]CuBr_4$	C_4CuBr	Cu—Br = 2.436 Å	[20]

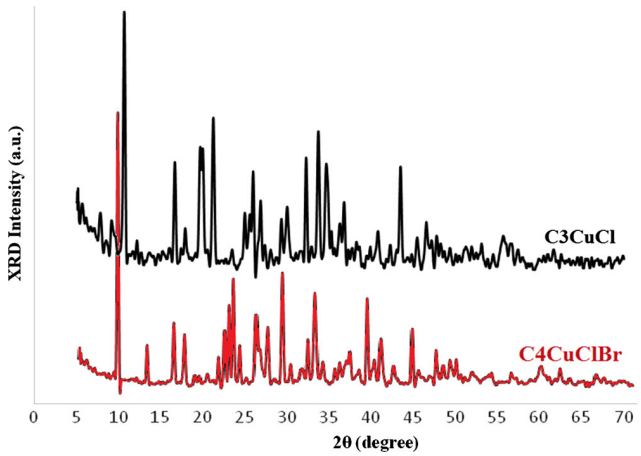

Figure 7. XRD diffraction patterns of C_3CuCl and $C_4CuClBr$.

3. Result and Discussion

3.1. Elemental Analysis

Microchemical analysis and SEM–EDX have been used to investigate the presence of each element in the synthesized perovskites after preparation. The carbon, nitrogen, and hydrogen percentages have been determined by microchemical analyses center in Cairo University. The calculated values according to the elemental molecular weight for (C, H, and N) divided by the total molecular weight for the compound. The calculated and measured results of all synthesized perovskites analysis are shown in **Table 1**.

The EDX spectra for C_3CuCl and $C_4CuClBr$ (apart from crystal images taken by computerized OPTIKA Microscopes B-190) are shown in **Figure 5** and **6**, respectively. The atomic percentage of metal and halide for all synthesized materials is tabulated in inset of each figure, which confirms the elemental composition of different metals and halides.

The results obtained by EDX may be due to instrumental limitations that make quantification of light elements such as C and N difficult. So, the main focus of the spectrum was the compositional analysis of the inorganic component of the perovskite, we investigated the variations of Cu, Cl, and Br. The O signal also be seen in the spectra may be attribute to water molecule. The shown data in microchemical analysis and EDX confirm the presence of all used elements in the preparation and the hybrids are in the correct chemical formula.

3.2. X-Ray Diffraction

The structure of Cu hybrid consists of corner shared octahedral structure anion followed by organic cations that form cations–anions–cations cohesions as discussed in detail in our previous work and other reported Cu hybrid perovskites.[7,12–14,25–29] **Table 2** shows the Cu—X, X = Cl, Br average bond length of short organic chain length of the formula $[(NH_3)(CH_2)_n(NH_3)]CuX_4$, $n = 2, 3, 4$.

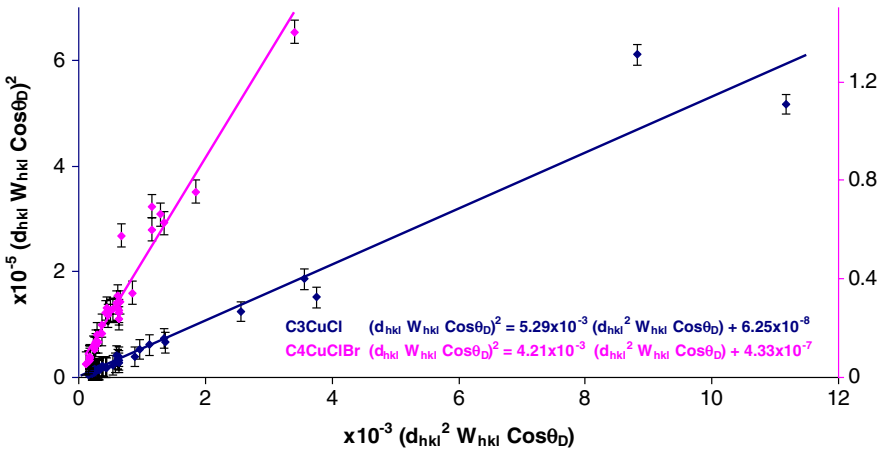

Figure 8. Linear fit of SSP of C_3CuCl and $C_4CuClBr$.

Table 3. The calculated values of crystallite size (nm) and microstrain by four methods of C_3CuCl and $C_4CuClBr$.

Compound	Debye–Scherrer	Williamson–Hall		Halder–Wagner		SSP	
	D [nm]	D [nm]	ε [10^{-4}]	D [nm]	ε [10^{-3}]	D [nm]	ε [10^{-3}]
C_3CuCl	29.01	42.33	0.99	38.66	0.58	38.82	0.5
$C_4CuClBr$	29.86	45.04	3.44	48.8	2.14	48.8	1.32

From this table, one can see that the Cu—Cl bond length is shorter than Cu—Br bond length by ≈0.14 Å regardless the organic chain length.

X-ray diffraction was used to evaluate the crystalline size of the obtained perovskite. The Debye–Scherrer's Equation (3) was used to determine the average crystalline size.

$$D = \frac{k\lambda}{W\cos\theta} \tag{3}$$

where k is the shape factor which usually takes a value of 0.94, W is the full width half maximum intensity (FWHM) in radians, λ is the used wavelength of the X-ray radiation ($\lambda_{Cu} = 1.54056$ Å), D is the average crystalline size, and θ is the Bragg diffraction angle. The XRD diffraction patterns of C_3CuCl and $C_4CuClBr$ shown in **Figure 7**, at $T = 298$ K.

In addition to Debye–Scherrer's method to determine the crystalline size, there are another methods to estimate D and the average lattice microstrain ε[32–36] can be also estimated from the Williamson–Hall's equation,[37–43] Halder–Wagner's method,[44–46] and size–strain plot (SSP) (linear fit is shown in **Figure 8**).[47,48] **Table 3** shows the calculated value of crystalline size and microstrain for synthesized perovskites at room temperature. The tunable crystal size, depending on the change in the length of the organic chain or the replacement of the halide, will have an effect on the optical properties (the next section).

It is clear that, all D value that calculated using Williamson–Hall, Halder–Wagner's method, and SSP techniques are higher than that obtained of Debye–Scherrer equation where these methods take into effect of all diffraction peaks and consider the lattice strain, which is missed in Scherrer's equation.[37–39]

Table 4. The assignment of the observed bands of IR for the compound $[(NH_3)_2(CH_2)_3]CuCl_4$ and $[(NH_3)_2(CH_2)_4]CuCl_2Br_2$.

Attributed to[a)]	C_3CuCl	$C_4CuClBr$
$\nu_{as}(NH_3)$	3429	3682, 3435
$\nu_s(NH_3)$	3032	3066, 3024
ν_{as} (CH_3)/The N–H···Cl bond	2942, 2712	2872, 2624
$\delta_{as}(NH_3)$	1574	1584
$\delta_s(NH_3)/\delta(CH_2)$	1495	1469
$\delta_w(CH_2)/\delta_t(CH_2)$	1395, 1146	1402, 1342
ν(C—C)/$r(NH_3)$	1050	1109, 1025
ν_{sy}(C—N)	875	915, 869
C—H_2 (δ_S)	808	757, 726
Tortional C—N	541, 496	496, 423
References	[16,23,24,51]	[16,17,51,52]

[a)]sy, symmetric; asy, asymmetric; ν, stretching; δ, bending; δ_w, wagging; r, rocking.

3.3. IR Spectroscopy

The infrared spectra of hybrid perovskites C_3CuCl, $C_4CuClBr$ are recorded at room temperature and shown in **Figure 9**. It is difficult to assign all bands to their source bonds, but the most important peaks are analyzed by comparison with similar compounds.

Also the vibrational study of infrared absorption has been carried out to get more information on the crystal structure. Figure 9 shows the infrared spectra of $[(NH_3)_2(CH_2)_3]CuCl_4$ and $[(NH_3)_2(CH_2)_4]CuCl_2Br_2$.

The absorption peak of 3000–3500 cm^{-1} is assigned to N—H stretching. The $\nu_{as}(NH_3)$ asymmetric stretching modes

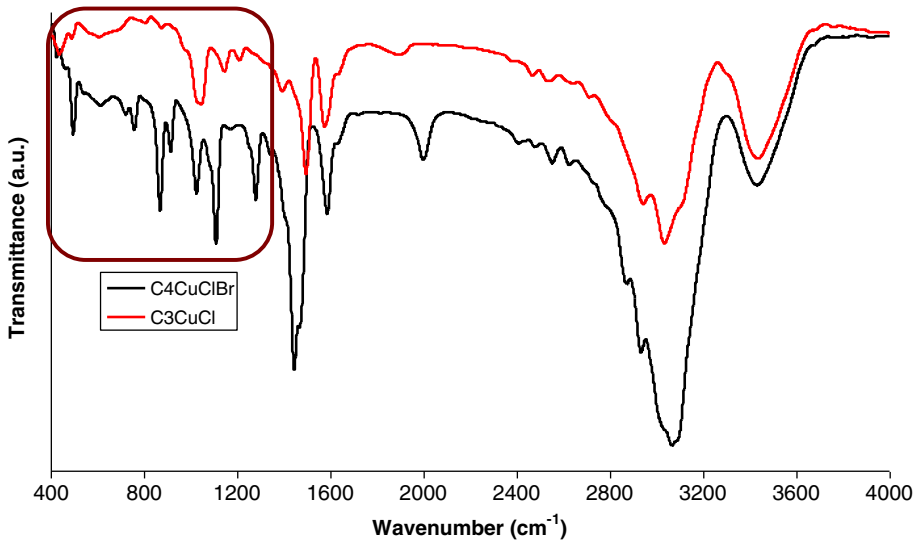

Figure 9. The infrared spectrum of the compounds $[(NH_3)_2(CH_2)_3]CuCl_4$ and $[(NH_3)_2(CH_2)_4]CuCl_2Br_2$ at room temperature.

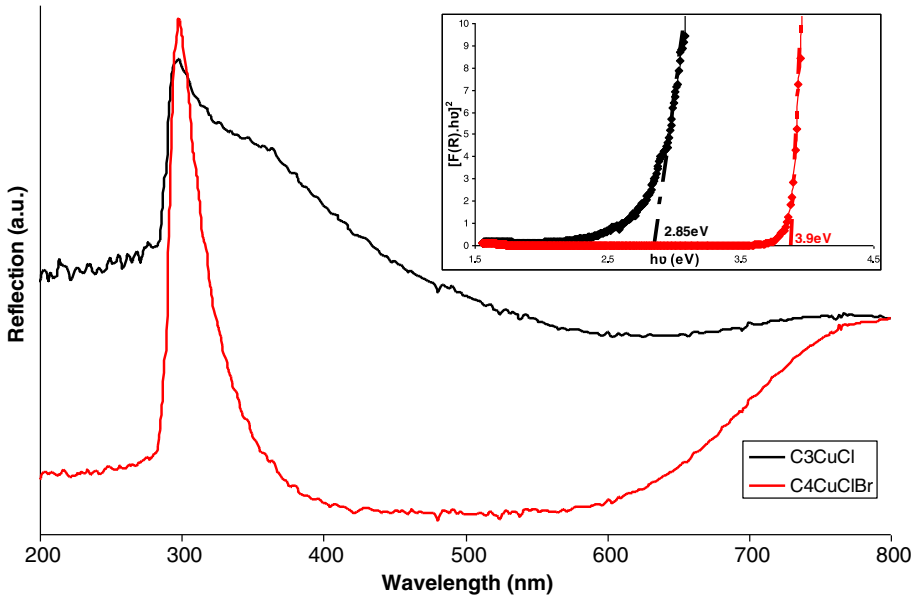

Figure 10. Optical properties of C_3CuCl and $C_4CuClBr$, the bandgap energy for C_3CuCl and $C_4CuClBr$ in the inset figure.

3500–3200 cm^{-1} and $\nu_s(NH_3)$ symmetric modes are assigned to peaks in range 3200–3500 cm^{-1}.[24] The $\nu_{as}(CH_2)$ asymmetric stretching mode appeared at 2900–2950 cm^{-1}. The hydrogen bonds are expected at 2950–2850 cm^{-1} band. The bands associated with CH stretching are in range 2780–2790 cm^{-1} and the nonfundamental NH and CH modes in the range 2600–1800 cm^{-1}.[49] Weak intensities peaks occurred at 2400–2600 cm^{-1} region, which are attributed to combination and overtone bands of N—H deformation modes and C—NH_3 torsion modes.[24] The CH_2 bending modes are associated with bands at 1490–1470 cm^{-1}. The asymmetric $\delta_{as}(NH_3)$ and symmetric $\delta_s(NH_3)$ bending modes are bands observed in the range 1450–1600 cm^{-1}. The C—N stretching modes are occurred around 860–1200 cm^{-1}, whereas 600–2100 cm^{-1} is assigned to C—C symmetric stretching.[50] The C—N torsional mode observed at the range of 550–400 cm^{-1}.[13]

The assignment of the bands in IR absorption is shown in **Table 4** for $[(NH_3)_2(CH_3)_2]CuCl_4$ and $[(NH_3)_2(CH_2)_4]CuCl_2Br_2$.

Figure 9 shows the region bounded by brown rectangle is the fingerprint of the each molecule and lies from 1300 to 400 cm^{-1}.

3.4. Optical Measurements

The relation between the absorption of the sample (K), reflectance (R_∞), and scattering (S) are correlated in Schuster–Kubelka–Munk (SKM) remission function.

$$F_{SKM}(R_\infty) = (1 - R_\infty)^2/2R_\infty = K/S \tag{4}$$

In the plot of $(F(R_\infty)\ h\upsilon)^n$ versus $(h\upsilon)$, the extrapolation of the drawn straight line estimate the energy gap E_g according to the Kubelka–Munk equation.

$$(F(R_\infty)h\upsilon)^n = A(h\upsilon - E_g) \tag{5}$$

where υ is the vibration frequency, A is a constant, h is the Planck constant, and E_g is bandgap. The type of transition is associated with the exponent n which takes values 1/2 or 3/2 for indirect transitions, and 2 or 3 for direct allowed.[50,53–57]

Figure 10 shows the optical properties of $[(NH_3)_2(CH_2)_3]CuCl_4$ and $[(NH_3)_2(CH_2)_4]CuCl_2Br_2$. Due to the strong absorption at the UV region of $[(NH_3)_2(CH_2)_4]CuCl_2Br_2$ sample it may find attractive applications as UV light photocatalysis. The estimated energy gap plot is shown in the inset figure of the $[(NH_3)_2(CH_2)_3]CuCl_4$ and $[(NH_3)_2(CH_2)_4]CuCl_2Br_2$ sample which equals to 2.85 and 3.9 eV, respectively.

The bandgap energy rises when mixed halide Cl_2Br_2 with a small chain length is used. The OIHPs' dielectric activities are related to their mechanical properties and demonstrate the impact of microstructure on the polarons.[58]

4. Conclusion

Cu hybrid perovskites diammonium series $[(NH_3)_2(CH_2)_3]CuCl_4$ and $[(NH_3)_2(CH_2)_4]CuCl_2Br_2$ are successfully prepared by the evaporation method. Microchemical analysis, EDX, XRD, and FTIR have been used to confirm the formation of the novel hybrid perovskites. The X-ray diffraction for $[(NH_3)_2(CH_2)_3]CuCl_4$ and $[(NH_3)_2(CH_2)_4]CuCl_2Br_2$ are carried out, and the average crystallite size calculated are 38.8 and 48.8 nm, respectively. These Cu-based hybrid perovskites show strong absorption in UV region according to the optical absorption study. The energy gap of C_3CuCl and $C_4CuClBr$ are equal to 2.85 and 3.9 eV, respectively.

Acknowledgements

The authors thank Academy of Scientific Research and Technology ASRT-NSFC cooperation project ID.3233 for fund.

Conflict of Interest

The authors declare no conflict of interest.

Data Availability Statement

Research data are not shared.

Keywords

crystalline sizes, halide perovskites, optical properties, organic–inorganic perovskites, X-ray diffraction

Received: January 20, 2021
Revised: March 22, 2021
Published online:

[1] V. M. Goldschmidt, *Naturwissenschaften* **1926**, *14*, 477.
[2] E. C. C. D. Souza, R. Muccillo, *Mater. Res.* **2010**, *13*, 385.
[3] H. Choi, J. Jeong, H.-B. Kim, S. Kim, B. Walker, G.-H. Kim, J. Y. Kim, *Nano Energy* **2014**, *7*, 80.
[4] V. D'Innocenzo, A. R. Srimath Kandada, M. De Bastiani, M. Gandini, A. Petrozza, *J. Am. Chem. Soc.* **2014**, *136*, 17730.
[5] T. Baikie, Y. Fang, J. M. Kadro, M. Schreyer, F. Wei, S. G. Mhaisalkar, M. Graetzeld, T. J. Whitec, *J. Mater. Chem.* **2013**, *A1*, 5628.
[6] F. Brivio, A. B. Walker, A. Walsh, *Appl. Mater.* **2013**, *1*, 042111.
[7] D. B. Mitzi, K. Chondroudis, C. R. Kagan, *IBM J. Res. Develop.* **2001**, *45*, 29.
[8] Z. V. Todres, *Organic Chemistry in Confining Media*, Springer, New York **2013**.
[9] Da-Wei Fu, Ji-Xing Gao, Wen-Hui He, Xue-Qin Huang, Yu-Hua Liu, Yong Ai, *Angew. Chem. Int. Ed. Engl.* **2020**, *59*, 17477.
[10] D. B. Mitzi, *J. Mater. Chem.* **2004**, *14*, 2355.
[11] T. Maris, G. Bravic, N. Chanh, J. Leger, J. Bissey, A. Villesuzanne, R. Zouari, A. Daoud, *J. Phys. Chem. Solids* **1996**, *57*, 1963.
[12] K. Halvorson, R. Willett, *Acta Crystallogr. Section C: Crystal Struc. Commun.* **1988**, *44*, 2071.
[13] M. F. Mostafa, A. A. Youssef, *Zeitschrift für Naturforschung* **2004**, *A59*, 35.
[14] B. Kundys, A. Lappas, M. Viret, V. Kapustianyk, V. Rudyk, S. Semak, Ch Simon, I. Bakaimi, *Phys. Rev.* **2010**, *B81*, 224434.
[15] Q. Li, S. Li, K. Wang, Z. Quan, Y. Meng, B. Zou, *J. Phys. Chem. Lett.* **2017**, *8*, 500.
[16] S. K. Abdel-Aal, A. S. Abdel-Rahman, *J. Electronic Mater.* **2019**, *48*, 1686.
[17] S. K. Abdel-Aal, G. Kocher-Oberlehner, A. Ionov, R. Mozhchil, *Appl. Phys.* **2017**, *A123*, 531.
[18] S. K. Abdel-Aal, *Solid State Ionics* **2017**, *303*, 29.
[19] M. F. Kandeel, S. K. Abdel-Aal, A. F. El-Sherif, H. S. Ayoub, A. S. Abdel-Rahman, *IOP Conf. Ser. Mater. Sci. Eng.* **2019**, *610*, 012063.
[20] S. K. Abdel-Aal, A. S. Abdel-Rahman, W. M. Gamal, M. Abdel-Kader, H. S. Ayoub, A. F. El-Sherif, M. F. Kandeel, S. Bozhko, E. E. Yakimovd, E. B. Yakimov, *Acta Crystallogr. B: Struc. Sci. Cryst. Eng. Mater.* **2019**, *75*, 880.
[21] S. K. Abdel-Aal, A. S. Abdel-Rahman, G. G. Kocher-Oberlehner, A. Ionov, R. Mozhchil, *Acta Crystallogr. A Found. Crystallogr.* **2017**, *70*, C1116.
[22] S. K. Abdel-Aal, A. S. Abdel-Rahman, *J. Cryst. Growth* **2017**, *457*, 282.
[23] M. S. Lassoued, M. S. Abdelbaky, A. Lassoued, R. M. Meroño, S. Ammar, A. Gadri, A. B. Salah, S. García-Granda, *J. Mol. Struct.* **2017**, *1141*, 660.
[24] H. Jeghnou, A. Ouasri, A. Rhandour, M.-C. Dhamelincourt, P. Dhamelincourt, A. Mazzah, P. Roussel, *J. Raman Spectrosc.* **2005**, *36*, 1023.
[25] A. A. Bunaciu, E. G. UdriŞTioiu, H. Y. Aboul-Enein, *Crit. Rev. Analyt. Chem.* **2015**, *45*, 289.
[26] J. K. Garland, K. Emerson, M. Pressprich, *Acta Crystallogr. C: Cryst. Struc. Commun.* **1990**, *46*, 1603.
[27] K. Pradeesh, G. S. Yadav, M. Singh, G. V. Prakash, *Mater. Chem. Phys.* **2010**, *124*, 44.
[28] W. Liu, J. Xing, J. Zhao, X. Wen, K. Wang, P. Lu, Q. Xiong, *Adv. Opt. Mater.* **2017**, *5*, 1601045.
[29] B. Cullity, S. Stock, in *Elements of X-ray Diffraction*, 3rd edn, Prentice Hall, New York **2001**, pp. 174–177.
[30] K. Tich, J. Bene, W. Hxlg, *Acta Crystallogr. B: Struc. Sci. Cryst. Eng. Mater.* **1978**, *34*, 2970.
[31] K. Halvorson, R. D. Willett, *Acta Crystallogr. C: Cryst. Struct. Commun.* **1988**, *44*, 2071.
[32] H. Hassan, D. Moubarak, J. Khaliel, H. Ayoub, A. Abdel-Rahaman, S. Khairy, T. El-Rasasi, Y. Elbashar, *Nonlinear Opt. Quantum Opt.* **2018**, *48*, 313.
[33] D. I. Moubarak, H. H. Hassan, T. Y. El-Rasasi, H. S. Ayoub, A. S. Abdel-Rahaman, S. A. Khairy, Y. Elbashar, *Nonlinear Opt. Quantum Opt.* **2018**, *49*, 295.
[34] D. I. Moubarak, J. A. Khaliel, T. Y. El-Rasasi, H. S. Ayoub, A. S. Abdel-Rahaman, S. A. Khairy, H. H. Hassan, Y. H. Elbashar, *Lasers Eng.* **2019**, *43*, 201.
[35] D. I. Moubarak, H. H. Hassan, H. S. Ayoub, T. Y. El-Rasasi, S. H. A. Khairy, Y. H. Elbashar, A. S. Abdel-Rahaman, *Lasers Eng.* **2019**, *43*, 319.
[36] D. I. Moubarak, H. H. Hassan, T. Y. El-Rasasi, H. S. Ayoub, A. S. Abdel-Rahaman, S. A. Khairy, Y. H. Elbashar, *Nonlinear Opt. Quantum Opt.* **2021**, *53*, 31.
[37] Y. Slimani, M. A. Almessiere, E. Hannachi, A. Baykal, A. Manikandan, M. Mumtaz, F. Ben Azzouz, *Ceram. Int.* **2019**, *45*, 2621.
[38] M. A. Almessiere, Y. Slimani, S. Güner, J. van Leusen, A. Baykal, P. Kögerler, *J. Mater. Sci.: Mater. Electron.* **2019**, *30*, 11181.
[39] S. K. Abdel-Aal, A. S. Abdel-Rahman, S. H. Ismail, *Egypt. J. Solids* **2019/2020**, *42*, 49.
[40] S. K. Abdel-Aal, A. S. Abdel-Rahaman, *J. Nanoparticle Res.* **2020**, *22*, 267.
[41] Y. H. Elbashar, R. A. Ibrahem, J. A. Khaliel, D. I. Moubarak, A. S. Abdel-Rahaman, A. H. H. Hassan, *Nonlinear Opt. Quantum Opt.* **2019**, *51*, 195.
[42] Y. H. Elbashar, W. A. Rashidy, J. A. Khaliel, D. I. Moubarak, A. S. Abdel-Rahaman, H. H. Hassan, *Nonlinear Opt. Quantum Opt.* **2019**, *51*, 171.
[43] Y. H. Elbashar, A. E. Omran, S. M. Hussien, M. A. Mohamed, R. A. Ibrahem, W. A. Rashidy, A. S. AbdelRahaman, H. H. Hassan, *Nonlinear Opt. Quantum Opt.* **2020**, *52*, 337.
[44] F. Izumi, T. Ikeda, in *Implementation of the Williamson–Hall and Halder–Wagner Methods into RIETAN-FP, Annual report*, Vol. *3*, Nagoya Institute of Technology, Aichi, Japan **2015**, pp. 33–38.
[45] D. Nath, F. Singh, R. Das, *Mater. Chem. Phys.* **2020**, *239*, 122021.
[46] T. Ida, S. Shimazaki, H. Hibino, H. Toraya, *J. Appl. Crystallogr.* **2003**, *36*, 1107.
[47] D. Balzar, H. Ledbetter, *J. Appl. Crystallogr.* **1993**, *26*, 97.
[48] V. D. Mote, Y. Purushotham, B. N. Dole, *J. Theor. Appl. Phys.* **2012**, *6*, 6.
[49] A. Ouasri, A. Rhandour, M.-C. Dhamelincourt, P. Dhamelincourt, A. Mazzah, *Spectrochim. Acta Part A: Mol. Biomol. Spectrosc.* **2003**, *59*, 357.

[50] H. Ferjani, H. Boughzala, *J. Mater.* **2014**, *2014*, 253602.
[51] M. F. Mostafa, S. S. Elkhiyami, S. A. Alal, *Mater. Chem. Phys.* **2017**, *199*, 454.
[52] P. Mondal, S. K. Abdel-Aal, D. Das, S. M. Islam, *Catal. Lett.* **2017**, *147*, 2332.
[53] H. Nikol, A. Vogler, *J. Am. Chem. Soc.* **1991**, *113*, 8988.
[54] H. Nikol, A. Becht, A. Vogler, *Inorg. Chem.* **1992**, *31*, 3277.
[55] A. Vogler, H. Nikol, *Pure Appl. Chem.* **1992**, *64*, 1311.
[56] A. Vogler, H. Nikol, *Comments Inorg. Chem.* **1993**, *14*, 245.
[57] C. Xiao, Z. Li, H. Guthrey, J. Moseley, Y. Yang, S. Wozny, H. Moutinho, B. To, J. J. Berry, B. Gorman, Y. Yan, K. Zhu, M. Al-Jassim, *J. Phys. Chem. C* **2015**, *119*, 26904.
[58] M. Catedral, A. Tapia, R. Sarmago, J. Tamayo, E. Del Rosario, *Sci. Diliman* **2004**, *16*, 41.